Peripheral Nerve Magnetoneurography With Optically Pumped Magnetometers

Yifeng Bu[1†], Jacob Prince[1†], Hamed Mojtahed[1], Donald Kimball[1], Vishal Shah[2], Todd Coleman[3], Mahasweta Sarkar[4], Ramesh Rao[1], Mingxiong Huang[5], Peter Schwindt[6], Amir Borna[6] and Imanuel Lerman[1,7,8]*

[1]Jacobs School of Engineering, Electrical and Computer Engineering, University of California San Diego, San Diego, CA, United States, [2]QuSpin Inc., Boulder, CO, United States, [3]Department of Bioengineering, Stanford University, Stanford, CA, United States, [4]Electrical and Computer Engineering Department, San Diego State University, Stanford, CA, United States, [5]Department of Radiology, Radiology Imaging Laboratory, University of California San Diego, San Diego, CA, United States, [6]Quantum Information Sciences, Sandia National Laboratories, Albuquerque, NM, United States, [7]Department of Anesthesiology, Center for Pain Medicine, University of California San Diego, San Diego, CA, United States, [8]Veterans Health Administration, VA San Diego, Center for Stress and Mental Health, San Diego, CA, United States

Electrodiagnosis is routinely integrated into clinical neurophysiology practice for peripheral nerve disease diagnoses, such as neuropathy, demyelinating disorders, nerve entrapment/ impingement, plexopathy, or radiculopathy. Measured with conventional surface electrodes, the propagation of peripheral nerve action potentials along a nerve is the result of ionic current flow which, according to Ampere's Law, generates a small magnetic field that is also detected as an "action current" by magnetometers, such as superconducting quantum interference device (SQUID) Magnetoencephalography (MEG) systems. Optically pumped magnetometers (OPMs) are an emerging class of quantum magnetic sensors with a demonstrated sensitivity at the 1 fT/$\sqrt{Hz}$ level, capable of cortical action current detection. But OPMs were ostensibly constrained to low bandwidth therefore precluding their use in peripheral nerve electrodiagnosis. With careful OPM bandwidth characterization, we hypothesized OPMs may also detect compound action current signatures consistent with both Sensory Nerve Action Potential (SNAP) and the Hoffmann Reflex (H-Reflex). In as much, our work confirms OPMs enabled with expanded bandwidth can detect the magnetic signature of both the SNAP and H-Reflex. Taken together, OPMs now show potential as an emerging electrodiagnostic tool.

Keywords: optically pumped magnetometer, magnetoneurography, magnetoencephalography, H-Reflex, sensory nerve action potentials, magnetospinography, super conducting quantum interference devices

INTRODUCTION

The human peripheral nervous system is composed of an intricate network of motor, sensory, and autonomic neural structures (Barr, 1974; Sulaiman et al., 2001; Mai and Paxinos, 2011) that if injured can result in peripheral neuropathic pain. Electrodiagnosis augments the clinicians' ability to gauge the severity of the neuropathy and the distribution of neuropathic dysfunction, that consequently guide clinical pharmacologic, minimally invasive, or invasive surgical interventions

(Do Campo, 2021). Well established in clinical neurophysiology practice, conventional (surface electrode) electrodiagnostics, routinely identify peripheral neuropathy and peripheral nerve entrapment with the Sensory Nerve Action Potential (SNAP); whereas plexopathy, demyelinating disease and radiculopathy are identified with the Hoffmann Reflex (H-Reflex). SNAP measures electrically evoked sensory nerve fiber action potentials of the upper and lower extremities; while the H-Reflex, an electrically evoked sensory-motor mono-synaptic spinal reflex, may be recorded from any surface muscle with an accessible nerve (Jabre and Stålberg, 1989; Burke et al., 1999). Abnormal (delayed 3–4 ms) H-Reflexes are known to occur at the onset of nerve root compression at the very early stage of nerve root injury even when imaging is normal and remains abnormal until the compression ceases (i.e., with selective nerve root injection or corrective surgical intervention; Jin et al., 2010; Zheng et al., 2014). Further, H-Reflexes are absent in acute inflammatory demyelinating polyneuropathy (Guillain–Barré syndrome; Bamford and Davis, 2020). Abnormal SNAP measures (delay or amplitude decrement) are regularly identified early in peripheral nerve entrapment and are pathognomonic in peripheral neuropathy (Krarup, 2004; Yang et al., 2021). Although surface electrode SNAP and H-Reflexes are proven integral electrodiagnostic measures, novel nascent magnetoneurography techniques are in development, capable of compound action current measurement in the peripheral nerve and muscle.

Super conducting quantum interference devices (SQUID) sensor arrays are a non-invasive diagnostic employed to detect cortical neuronal action potentials with magnetoencephalography (MEG). Peripheral nerve action currents in the human upper extremity (median and ulnar nerve; termed magnetoneurography; Hari et al., 1989; Hashimoto et al., 1994; Lang et al., 1998) and, more recently, in the dorsal root ganglion and spinal cord (termed magnetospinography) have successfully been detected with SQUID sensor arrays (Adachi et al., 2009). However, conventional SQUID sensor use is highly limited, as they require cryogenic temperature provided with liquid helium (4 K or −269°C) and magnetically shielded rooms (MSRs). Moreover, SQUID sensors are housed in a rigid Dewar which prohibit adjacent placement to the sensory, motor nerve, or the target muscle that inherently requires highly mobile and conformal sensor arrays.

QuSpin OPM sensors are conformal with a 6.5 mm sensor stand-off that in aggregate contribute to an improved magnetic signal-to-noise ratio therefore capable of surpassing current SQUID sensor technology due to closer proximity to the neuronal source (Iivanainen et al., 2017; Hill et al., 2020). Recently, Broser et al. (2018, 2020) showed that commercial Gen-1 OPMs (QuSpin Inc., CO, United States) detect compound muscle action currents consistent with motor neuron activation. Expounding on this work, we employed the commercially available Gen-2 OPM (QuSpin Inc., CO, United States) with the aim to measure upper extremity action currents equivalent to the SNAP and H-Reflex. To achieve this aim we meticulously: (1) characterized the frequency response, phase response, and sensitivity of the OPM sensor, and (2) validated the temporal resolution of the OPM's recording of upper extremity action

currents (equivalents of SNAP and H-Reflex) when equated to conventional surface electrodes. In concert, these results demonstrate preliminary potential for OPM as a peripheral nerve electrodiagnostic tool.

MATERIALS AND METHODS

OPM Operational Bandwidth

QuSpin Gen2 OPMs were used to measure median nerve compound action currents. In comparison to the Gen-1 OPM (dimensions: $13.0 \times 19.0 \times 110.0\,mm^3$), Gen-2 OPMs have a significantly smaller footprint ($12.4 \times 16.6 \times 24.4\,mm^3$) that improves conformal placement of the OPM array. Gen-2 OPMs demonstrate improved sensitivity (7–$10\,fT/\sqrt{Hz}$ in ideal conditions) and have an extended tolerance to background magnetic field (up to 200 nT) while maintaining ±5 nT dynamic range (Shah and Romalis, 2009). The OPM integrates a sixth-order digital filter at 500 Hz to eliminate residual response above this frequency.

QuSpin OPM sensor response capability of magnetic field frequencies (up to 500 Hz) was identified with response to a frequency chirp function. The voltage chirp function (swept linearly from 1 Hz to 700 Hz over a 2 s period) was converted into a proportional magnetic chirp by a copper-wire Helmholtz Coil (two 7.5 cm radius loops with five coils per loop at 7.5 cm separation) and associated current supply circuit (**Supplementary Figure 1**). Based on electromagnetic theory, the amplitude of the current running through the Helmholtz coil is directly proportional to the amplitude of the magnetic field generated at the center of the two coils (Bronaugh, 1995; Wang et al., 2002; Cvetkovic and Cosic, 2007; de Melo et al., 2009). Accordingly, the current supply was controlled to generate a 600 pT peak-to-peak (pk-pk) alternating magnetic field at the OPM's central location. Using the OPM recordings of repeated ($N=11$) chirp functions, the OPM magnitude and phase response were then calculated. Additionally, the sensitivity of the sensor was calculated by computing the power spectral density of an empty room recording and dividing this value by the normalized frequency response curve. Before the creation of the sensitivity plot, the OPM signal was filtered for powerline sources (i.e., 60 Hz and its harmonics) that allowed for removal of these sensitivity spikes. Finally, using the same Helmholtz Coil setup with a varying input current amplitude, the OPM response to a 73 Hz sinusoidal magnetic field input was recorded at amplitudes measured between 15 and 1,500 pT. Magnetic recordings from this experiment were used to calculate the total harmonic distortion of the OPM at multiple measured signal amplitudes.

Experimental Setup and Procedures

The Institutional Review Board at the University of California San Diego (UCSD) Health Systems approved the experimental protocol (UCSD IRB: 171154). Three healthy male subjects (age: 40 ± 12 years) without history, signs, or symptoms of peripheral neuropathy, nerve entrapment syndrome or radiculopathy, gave their written consent. On the visit day,

surface electrode and OPM-based peripheral nerve measurements were carried out within the UCSD Radiology Imaging Laboratory's six-layer MSR (IMEDICO, Switzerland) to minimize the effects of powerline noise and the Earth's magnetic field. The employed MSR has a shielding factor of 65–160 dB for the 0.01–10 Hz frequency range. Subjects were asked to remove all electronic equipment and metal accessories before entering the MSR to avoid magnetic noise and sensor saturation.

Median Nerve Sensory Nerve Action Potential and Current Measure

The subject ($N = 1$) was centered in the middle of the MSR in the supine position. A pillow was positioned below the subject's left elbow to ensure comfortable yet maximal extension of the upper arm above the head. The median nerve SNAP and sensory nerve action current were measured between the brachialis and the biceps brachii. A 20 MHz portable ultrasound transducer (Butterfly IQ, Palo Alto, United States) was used to measure the median nerve depth, circumference, and area at both proximal bicep and distal bicep sites. Stimulating electrodes with cathode–anode distance of 1.5 cm were secured (with a Velcro strap) longitudinally over the left median nerve at the wrist with cathode proximal to anode. Two pairs of active and reference electrodes were localized (*via* ultrasound image guidance) over the median nerve separated by a 2 cm, 4 cm, and 6 cm distance while the ground electrode was placed between the stimulator and the active electrode (**Figure 1A**). In all measurements, the skin was carefully abraded with the Nuprep skin prep gel (Weaver and Company, CO, United States) and the EC3 Grass conductive adhesive gel (Natus, Pleasanton, CA, United States) was applied to each electrode cup with assurance of impedance maintenance at 5,000 Ω or less. Subjects

then underwent left median nerve supramaximal stimulation with the DS7AH constant stimulator (Digitimer Ltd., United Kingdom) using a 0.23 Hz, 500 μs pulse-width, monopolar square-wave.

Median Nerve Hoffman Reflex

The H-reflex response was elicited in the Flexor Carpi Radialis muscle (FCR) by stimulator placement along the antecubital fossa longitudinal axis directly over the left median nerve on two subjects. The recording techniques employed for H-Reflex generally followed the methodologies of two studies (Christie et al., 2005; Khosrawi et al., 2018). Briefly, the active electrode was placed over the muscle belly of the FCR located one-third of the distance between the medial epicondyle and radial styloid while the reference electrode was placed over the FCR tendon insertion site at the wrist (**Figure 2A**). Isometric contraction of the FCR muscle was used to facilitate the reflex response. Stimulation intensity was incrementally increased by 0.2 mA until a clear H-Reflex was elicited and, upon subsequent intensity increase, a reduction of H-Reflex amplitude with maximal M-wave was observed (Stowe et al., 2008).

To match surface electrode time-locked measurements of the SNAP and the H-Reflex, a single OPM was positioned (with conformal Velcro strap) at the identical sites of the active electrode (at either the proximal or distal site) in the above experiments (**Figures 1E, 2D**). In all measures, the z-direction of the OPM was adjusted normal to the skin surface in the longitudinal direction along the nerve. The *y*-axis of the OPM was used for measurement and the OPM was operated in single-axis mode.

To further confirm the source of the detected signals and to measure the spatial fall-off of the H-Reflex, 3 OPM sensors
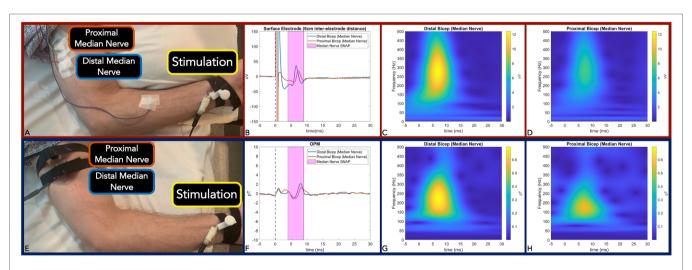

FIGURE 1 | Panel **(A,E)**: Measurement setup of Median nerve SNAP with surface electrode **(A)** and equivalent action current by OPM **(E)**. Panel **(B,F)**: Time-locked average comparison (from two sites: distal bicep = blue line; and proximal bicep = red line) between surface electrode (6 m inter-electrode distance) **(B)** and OPM **(F)** demonstrate identical 0.8 ms temporal dispersion for both modalities. SNAP action potential/currents are marked in the magenta shaded area. Panel **(C,D)**: Surface electrode time-frequency analysis for SNAP measured at the distal bicep **(C)** and proximal bicep **(D)**. Panel **(G,H)**: OPM time-frequency analysis for SNAP measured at distal bicep **(G)** and proximal bicep **(H)**. (OPM, Optically pumped magnetometers, SNAP, Sensory nerve action potential, μv, microvolt, pT, picoTesla, and ms, milliseconds).
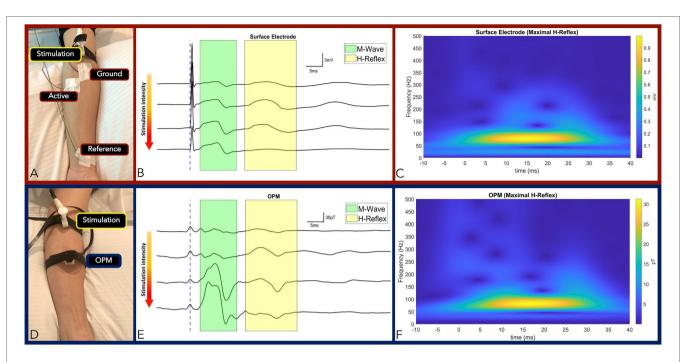
FIGURE 2 | Panel **(A,D)**: Measurement setup of FCR M-wave and H-Reflex responses measured by surface electrode **(A)** and OPM **(D)** from the same subject. Panel **(B,E)**: Time-locked averages with incremental increase in stimulation intensity from top to bottom traces by surface electrode **(B)** and OPM **(E)**. The M-wave and the H-Reflex responses are highlighted green and yellow, respectively. Conserved standard M and H-Reflex characteristics: (1) M-wave amplitude increased incrementally until a maximum was reached, while (2) H-Reflex amplitudes increased incrementally before reaching a maximum and subsequently decreasing and subsequently decreasing, were observed in all measurements (surface electrodes in B and OPM in E). Panel **(C)**: Surface electrode time-frequency analysis of FCR M-wave and maximal H-Reflex recorded. Panel **(F)**: OPM time-frequency analysis of FCR M-wave and maximal H-Reflex recorded. (OPM, Optically pumped magnetometers, FCR, Flexor carpi radialis, mV, millivolt, pT, picoTesla, ms, milliseconds, and TF, Time frequency).

were placed in transverse orientation to the FCR at the one-third (proximal FCR) and one-half (distal FCR) distance between the medial epicondyle and radial styloid (**Figures 3A,B**). The proximal and distal OPM sensors were separated longitudinally by 4.5 cm. The central OPM sensor was placed directly over the FCR muscle. At the equipotential level, the two remaining OPMs were positioned radially 0.5 cm lateral and medial to the central OPM sensor.

Processing Pipeline

The recorded surface electrode signal was amplified and bandpass filtered from 3 to 1,000 Hz using a Digitimer D360 isolated amplifier (Digitimer Ltd., United Kingdom) with a gain setting of 1,000 for SNAP measurement and 200 for H-Reflex measurement (Christie et al., 2005). The signal was sampled by a CED Micro1401 device at 10 kHz and recorded by Signal 8.19a software (Cambridge Electronic Design, Cambridge, United Kingdom). All stimuli were repeated with a time-locked trigger to enable trial averaging while no trial rejection was necessary due to high signal-to-noise ratio.

Prior to OPM Neuronal recordings, each OPM was tuned and calibrated in an absolute zero magnetic field environment in the closed door MSR with the OPM gain set to 2.7 V/nT. Of note, the OPM sixth-order hardware digital filter at 500 Hz is known to generate up to a 15 ms ringing effect post-electric stimulation (**Supplementary Figure 3**). In our measurements,

stimulation artifact was post-calibrated to 0 s to eliminate intrinsic OPM and analog digital converter delay. To reduce ringing effect data contamination, both stimulation artifact and subsequent ringing effect curves were regressed as a sinc function by non-linear least squares method and subtracted from the averaged data. A second order 20–500 Hz bandpass filtered was then applied. All post-processing was carried out with MATLAB software (MathWorks Inc., MA, United States). The same processing technique was applied on all physiological OPM measurements. To compare OPM and surface electrode neural signal bandwidth, time-frequency analysis (1–500 Hz) was computed by convolving the time-locked averaged data with complex Morlets' wavelet (Kronland-Martinet et al., 1987) as prior described by Cohen (2014).

RESULTS

OPM Frequency Response and Sensitivity

The averaged OPM normalized magnitude response (over 11 chirps) decreased as frequency was incrementally increased (**Figure 4A**). For the bandwidth between 1 Hz and 135 Hz (**Figure 4A** green shaded area), the magnitude response decreased minimally. Above 135 Hz, the magnitude response moderately decreased, and a reduced response was recorded up 500 Hz (**Figure 4A** yellow shaded area). Above 500 Hz, a large reduction
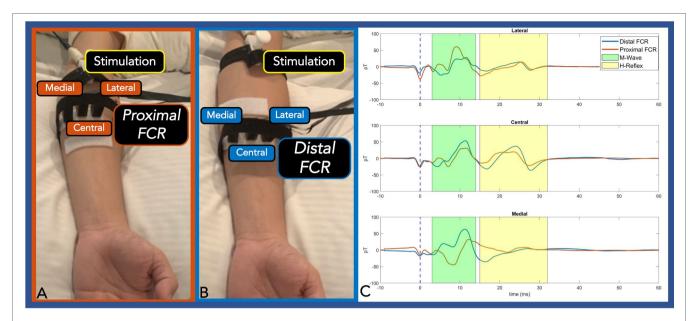
FIGURE 3 | Panel **(A,B)**: Three OPMs were transversely placed at an equipotential level on the proximal FCR **(A)** and distal FCR **(B)**. Panel **(C)**: The centrally placed OPM (directly over the FCR) exhibited the largest H-Reflex pk-pk amplitude compared with the two radially placed OPM sensors. At the proximal FCR, the lateral and the medial OPM showed reverse polarity. At the distal FCR, where the muscle spindle is thinner, the medial OPM only detected M-Wave activity. The M-wave and the H-Reflex responses are highlighted green and yellow, respectively. (OPM, Optically pumped magnetometers, FCR, Flexor carpi radialis, pT, picoTesla, and ms, milliseconds).
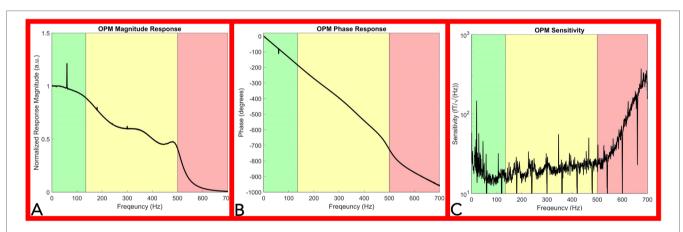

FIGURE 4 | OPM frequency response and sensitivity characterization. Panel **(A)**: Magnitude Response of the OPM. The OPM magnitude response decreased minimally up to 135Hz (green shaded area). A moderate reduction in response was recorded up to 500Hz (yellow shaded area). Above 500Hz, a large reduction in response is noted as a direct effect of the Gen2 OPM hardware digital filter in the electronic module (red shaded area). Panel **(B)**: Phase response of the OPM. OPM Phase response is approximately linear up to 500Hz (green and yellow shaded area). Panel **(C)**: Sensitivity response of the OPM. OPM sensitivity was divided into three segments: below 135Hz (green shaded area), from 135 to 500Hz (yellow shaded area), and from 500 to 700Hz (red shaded area). A rapid decrease in sensitivity is noted above 500Hz. (OPM, Optically pumped magnetometer, Hz, Hertz, and fT, femtotesla).

in response is noted as a direct effect of the Gen2 OPM hardware digital filter in the electronic module (**Figure 4A** red shaded area). Major spikes at multiples of 60 Hz in both the magnitude response and phase response plot (**Figures 4A,B**) are a result of the powerline noise and its harmonics.

The OPM phase response curve is approximately linear up to 500 Hz (**Figure 4B** green and yellow shaded area), indicating a relatively constant phase delay across these frequencies. A direct calculation of the average phase delay from 5 to 500 Hz

is 3.77 ± 0.078 ms. In our neurophysiological measurements below, we eliminated the delay introduced by this phase response by setting the start of the stimulation artifact to time zero, so that the temporal characteristics of our OPM measurements could be directly compared to the electrode measurements.

The OPM sensitivity was divided into three segments: below 135 Hz (**Figure 4C** green shaded area), from 135 to 500 Hz (**Figure 4C** yellow shaded area), and from 500 to 700 Hz (**Figure 4C** red shaded area). Ignoring outlier frequencies caused

by powerline and other technical noise sources, our measured sensitivities in the three segments are as: 17.7 ± 3.5 fT/$\sqrt{\text{Hz}}$ below 135 Hz, 20.8 ± 3.8 fT/$\sqrt{\text{Hz}}$ from 135 to 500 Hz, and 101.6 ± 85.6 fT/$\sqrt{\text{Hz}}$ above 500 Hz. Filtering at 60 Hz and its harmonics aimed to remove powerline noise inherently resulted in downward spikes at multiples of 60 Hz while environmental noise sources lowered sensitivity below 65 Hz (**Figure 4B**). The OPM total harmonic distortion ranged from −25 dBc to −60 dBc for measured input amplitudes between 15 and 1,500 pT.

Ultrasound Neural Imaging Measurements

Using high resolution B-mode ultrasound imaging, we accurately measured the median nerve circumference, area, and depth at the distal bicep and proximal bicep. The median nerve at two measurement sites was similar in circumference (1.72 cm and 1.7 cm, respectively) and area (0.21 cm^2 for both) but was located deeper at the proximal bicep (0.64 cm) when compared to the distal bicep (0.43 cm), (**Supplementary Figure 4**).

Optically Pumped Magnetometer Electrodiagnostic Measurements

Sensory Nerve Action Potential and Current

We first verified OPM-based detection of afferent sensory nerve action current when compared to surface electrode SNAP in the median nerve. We observed identical surface electrode and OPM 0.8 ms peak latency temporal dispersion (**Figures 1B,F**). We also calculated a nerve conduction velocity of 50 m/s, which is largely in line with reported median nerve (large fiber) orthodromic sensory conduction velocities (Shehab, 1998; Valls-Sole et al., 2016). Additionally, surface electrode (inter-electrode distance of 6 cm) action potential (time frequency derived) center frequencies were largely equivalent (260 Hz) when compared to OPM (200 Hz; **Figures 1C,D,G**). Of note, surface electrode (inter-electrode distance of 2 cm and 4 cm) action potential (time frequency derived) center frequencies (460 Hz and 300 Hz) were greater than the OPM center frequency (**Supplementary Figure 2**).

The effective current density of the nerve was simulated and back-calculated by the Biot-Savart magnetic MATLAB toolbox (Loic, 2015) by employing the detected B-field action current and median nerve-depth-to-vapor-cell distance (including the 6.5 mm sensor stand-off). The nerve was simulated as a straight wire. The estimated total current was 0.195 µA and 0.19 µA from the median nerve at proximal and distal bicep, respectively. The current density was calculated as 0.92 µA/cm^2 and 0.90 µA/cm^2 at the proximal and distal bicep, respectively.

Flexor Carpi Radialis Hoffman Reflex

Two experiments were conducted to verify accurate OPM-based detection of M-wave and H-Reflex of the FCR muscle. In our first experiment, stimulation intensity was gradually increased to elicit conserved standard M and H-Reflex characteristics: (1) M-wave amplitude increased incrementally with increasing stimulation intensity until a maximum amplitude was reached, while (2) H-reflex amplitudes increased incrementally with increasing stimulation intensity before reaching a maximum

and subsequently decreasing (**Figures 2B,E**). We compared the electromyography response and the reflex reaction of the FCR muscle between the gold standard surface electrode measures and the OPM. In subjects ($N=2$), we observed conserved standard M and H-Reflex characteristics with stimulation intensity increases in all measurements (OPM and surface electrodes). M-Wave (3.1 ms) and H-Reflex (17.6 ms) onset latencies were identical for surface electrode and OPM measurements (**Figures 2B,E**; **Supplementary Table 1**). M-wave and H-Reflex time-frequency analysis center frequency of 80 Hz was highly conserved across OPM and surface electrode measurements (**Figures 2C,F**) and M-wave general shape was conserved (Merletti et al., 1995).

In the second experiment, three radially placed OPMs were positioned at the one-third (proximal FCR) and one-half (distal FCR) distance between the medial epicondyle and radial styloid. At the proximal FCR, all three OPM successfully detected M-wave and H-Reflex activities. The central OPM had the largest H-Reflex pk-pk amplitude among the three measurements and the medial OPM showed reversed polarity. At the distal FCR, where the muscle spindle gets thinner, the central OPM measurements again showed larger H-Reflex activities compared with the lateral sensor. The medial OPM that was placed closer to the palmaris longus muscle only detected muscle activity (**Figure 3C**).

DISCUSSION

Widely adopted by clinical Neurophysiologists, conventional surface electrode electrodiagnostic measures (i.e., SNAP and H-Reflex) are routinely deployed to measure functional and dysfunctional neural physiology. Our work demonstrates, QuSpin Gen2 OPM can measure frequencies up to 500 Hz with a sensitivity capable of action current detection (SNAP and H-Reflex equivalent) confirmed with conventional surface electrode measures.

The presented frequency response curve and frequency-dependent sensitivity (**Figure 4**) indicate that the OPM sensor can measure frequencies: (1) above the reported bandwidth (135 Hz) and (2) within range of peripheral nerve action current frequencies (up to 500 Hz), but (3) with a reduced sensitivity in this range (135–500 Hz). Generally, the sensitivity of the OPM from 0 to 500 Hz is below 30 fT/$\sqrt{\text{Hz}}$ (**Figure 4C**). A 30 fT/$\sqrt{\text{Hz}}$ threshold of detection is well below the magnetic nerve action current signals detected throughout the study, which were on the range of or greater than one pT (1,000 fT). As such, the evoked magnetic activities observed throughout this report are above the minimum detection amplitude of the commercially available Gen2 OPM sensor and within its current capabilities.

The OPM linear phase response (between 0 and 500 Hz) indicates preservation of the phase relationships of different frequency components below 500 Hz necessary for peripheral nerve action current detection (**Figure 4B**). The observed nominal total OPM harmonic distortion (less than −25 dBc) indicates physiologic signals do not significantly distort nerve action current measures.

After sensor characterization, OPM fast fiber sensory nerve action current detection was confirmed with conventional surface electrode measurements. Identical SNAP temporal dispersion was measured using both surface electrodes and OPM. In both sensors, temporal dispersion derived nerve conduction velocities match expected large fiber 50 m/s conduction velocity. To our knowledge, this is the first measure of peripheral nerve action current with OPM.

It should be noted that with 6 cm surface electrode separation center frequencies of the action potential and action current were largely equivalent albeit with a nominal 60 Hz difference (**Figures 1C,D,G,H**). But with decreased surface inter-electrode distance (4 cm and 2 cm active to reference), we observed an incrementally increased action potential width and action current center frequency difference (100 Hz at 4 cm and 260 Hz at 2 cm) when compared to OPM (**Supplementary Figure 2**). These differences are due to a combination of factors. Because it takes a finite time (0.8 ms) for a peripheral large fiber SNP to travel from onset to maxima, the traveling action potential spatial distribution is calculated as approximately 4 cm with a concomitant nerve conduction velocity of 50 m/s (Dumitru et al., 2010). To accurately measure the full action potential signal, a minimum of 4 cm inter-electrode distance is required. But the closer the electrodes are placed (less than 4 cm), the more of the signal will be eliminated and hence the smaller it will appear (i.e., action potential amplitude and duration; Dumitru et al., 2010). In line, we detected a decrease in surface electrode center frequency with larger inter-electrode distances (460 Hz at 2 cm, 300 Hz at 4 cm, and 260 Hz at 6 cm; **Supplementary Figure 2**; **Figures 1C,D**). Precisely positioned over the active electrode site, the OPM acts as a single sensor with a fixed effective distance (i.e., circumferential diameter at which the median nerve propagating action current is detected) that likely contributes to the observed 200 Hz center frequency. In addition to the OPM fixed effective distance that potentially widened the action current, the qualitative amplitude reduction of high frequency action current components is most likely due to the OPM's intrinsic low pass filter, but other as yet identified factors may also contribute. Nonetheless, the OPM was capable of peripheral nerve action current detection (albeit with reduced response) that *invariably* preserved the equivalent (0.8 ms) surface electrode derived temporal dispersion. In sum, OPM accurately measures sensory nerve action current latency; however, the above-described factors may result in relative amplitude blunting due to a fixed effective distance, intrinsic sensitivity, qualitative filtering, and other undetermined factors. When considering OPM sensory nerve action current measures as a clinical diagnostic adjuvant, further work is essential in clinical disease populations (i.e., axonal neuropathy) where relative amplitude comparison between upper, lower, right, and left limbs is requisite.

Of note, the signals from surface electrodes and OPM are similar because they fundamentally arise from the same moving source (i.e., the median nerve propagating action potential or current). However, there are important distinctions. The OPM magnetometer measures the field vector while the surface measures a scalar quantity. Inherently, more information is captured (i.e., direction of the field) with OPM when compared to electrodes that may improve nerve action source localization with expanded ($N=10$) OPM sensor arrays. Moreover, we observed equivalent current densities: (1) 0.92 µA/cm^2 (0.64 cm median nerve depth at proximal position) and (2) 0.90 µA/cm^2 (0.43 cm median nerve depth at distal position) that in aggregate evince a capability to identify depth independent median nerve action currents. In the near future, OPM depth independent current density equivalents may: (1) expedite peripheral nerve source localization and peripheral nerve differentiation critical for both neural recording as well as targeted stimulation and (2) may supersede spatial resolution obtained with conventional electrode based finite element modeling. Clinically, (if developed) these depth independent current density algorithms may better identify neural root, trunk, division, cord, and branch dysfunction in plexopathies where multiple neural structures are in close proximity.

Analogous to SNAP measures, OPM M-wave and H-Reflex recordings were verified when compared to gold standard surface electrode measures. Time-locked OPM derived M-wave and H-reflex responses demonstrated the same temporal latency and center frequency when compared to those from the surface electrode measurements. Additionally, as we increased the stimulation amplitude, we observed an initial increase and then decrease in the H-Reflex amplitude, highly characteristic of an H-Reflex signal (Christie et al., 2005; Stowe et al., 2008).

Next, we identified a maximal peripheral FCR H-Reflex current source by distributing three separate OPM sensors within an equipotential line at both proximal and distal FCR. At both transverse levels, the centrally placed OPM (directly over the FCR) exhibited the largest H-Reflex pk-pk amplitude compared to the two radially placed OPM sensors. At the proximal FCR site, the lateral and medial OPM showed reverse polarity, demonstrating the propagation direction and the center location of the propagating action current. Collectively, this location dependent pattern of OPM signal magnitude (i.e., largest H-Reflex action current identified with Central OPM sensor placed directly over the FCR) supports peripheral nerve action current identification with OPM multi-sensor array methodology. Reliability of conventional FCR H-Reflex identification is low (Christie et al., 2005). Based on these preliminary results, OPM arrays distributed over the forearm area (4–10 OPMs) may expedite and improve reliable and objective identification of the FCR H-Reflex response.

Similar to single sensor, multi-OPM peak latencies were measured within typical range of conventional gold standard surface electrode FCR H-Reflex latency (17–18 ms; Jabre, 1981; Christie et al., 2005; Khosrawi et al., 2018). Future clinical cohort studies are planned in patients with known demyelinating disease, plexopathy, or radiculopathy with the aim to identify pathological absent or slowed H-Reflex measured with OPM.

While our OPM action current recordings are encouraging, our work is not without limitations. First, the OPM is only operational within a MSR which limits general use in the open conventional clinic setting. Future work will focus on the development of open field capable small single limb (arm or leg) magnetic shielding devices that may afford convenient

in office OPM electrodiagnostic (SNAP and H-Reflex) characterization that inherently may lower costs when compared to conventional MSR. Second, post-hoc stimulation artifact and ringing effect removal were required to obtain early SNAP measures. Future automated optimization of OPM filtering techniques applied to the transimpedance amplifier interaction with the lock-in amplifier is planned; this may minimize the ringing effect. Additionally, accurate OPM neuronal action potential measurement requires informed placement of each sensor, i.e., B-mode median nerve and Flexor Carpi Radialis imaging. Employing a multiarray 4–10 OPM sensor solution has the potential to circumvent the requirement for B-mode ultrasound scanning and therefore may improve SNAP and FCR H-Reflex reliability. As prior mentioned, OPM intrinsic sensitivity and filtering may result in amplitude blunting of fast component sensory nerve action currents. Future clinical cohort studies may define OPM sensory nerve action current amplitude characteristic accuracy and reliability as a clinical electrodiagnostic.

In summary, we demonstrate two major findings: (1) the commercially available QuSpin Gen2 OPM is capable of measuring signals at a frequency above 135 Hz (up to 500 Hz) with a sensitivity and phase response appropriate for the detection of peripheral nerve action current (SNAP and H-Reflex) equivalents and (2) OPM has comparable temporal resolution to gold standard surface electrodes when measuring SNAP and H-Reflex equivalents. Taken together, our results warrant further OPM sensor electrodiagnostic investigation in clinical disease cohorts.

DATA AVAILABILITY STATEMENT

Data is available at the author's discretion upon direct request.

REFERENCES

Adachi, Y., Kawai, J., Miyamoto, M., Ogata, H., Tomori, M., Kawabata, S., et al. (2009). A SQUID system for measurement of spinal cord evoked field of supine subjects. *IEEE Trans. Appl. Supercond.* 19, 861–866. doi: 10.1109/TASC.2009.2019199

Bamford, J. A., and Davis, S. F. (2020). "The H-reflex and F-response," in *Principles of Neurophysiological Assessment, Mapping, and Monitoring* (Switzerland: Springer), 171–179.

Barr, M. L. (1974). *The Human Nervous System: An Anatomical Viewpoint.* New York: Harper & Row.

Bronaugh, E. L. (1995). "Helmholtz coils for calibration of probes and sensors: limits of magnetic field accuracy and uniformity," in *Proceedings of International Symposium on Electromagnetic Compatibility: IEEE*, 72–76.

Broser, P. J., Knappe, S., Kajal, D.-S., Noury, N., Alem, O., Shah, V., et al. (2018). Optically pumped magnetometers for magneto-myography to study the innervation of the hand. *IEEE Trans. Neural Syst. Rehabil. Eng.* 26, 2226–2230. doi: 10.1109/TNSRE.2018.2871947

Broser, P., Middelmann, T., Sometti, D., and Braun, C. (2020). Optically pumped magnetometers disclose magnetic field components of the muscular action potential. *J. Electromyograph. Kinesiol.* 56:102490. doi: 10.1016/j.jelekin.2020.102490

Burke, D., Hallett, M., Fuhr, P., and Pierrot-Deseilligny, E. (1999). H reflexes from the tibial and median nerves. The International Federation of Clinical Neurophysiology. *Electroencephalogr Clin Neurophysiol Suppl.* 52, 259–262.

Christie, A. D., Inglis, J. G., Boucher, J. P., and Gabriel, D. A. (2005). Reliability of the FCR H-reflex. *J. Clin. Neurophysiol.* 22, 204–209. doi: 10.1097/01. WNP.0000162376.16773.A8

Cohen, M. X. (2014). *Analyzing Neural Time Series Data: Theory and Practice.* London: MIT press.

Cvetkovic, D., and Cosic, I. (2007). "Modelling and design of extremely low frequency uniform magnetic field exposure apparatus for in vivo bioelectromagnetic studies," in *2007 29th Annual International Conference of the IEEE Engineering in Medicine and Biology Society: IEEE*, 1675–1678.

De Melo, C. F., Araújo, R. L., Ardjomand, L. M., Quoirin, N. S. R., Ikeda, M., and Costa, A. A. (2009). Calibration of low frequency magnetic field meters using a Helmholtz coil. *Measurement* 42, 1330–1334. doi: 10.1016/j. measurement.2009.04.003

Do Campo, R. V. (2021). Electrodiagnostic assessment of polyneuropathy. *Neurol. Clin.* 39, 1015–1034. doi: 10.1016/j.ncl.2021.06.012

Dumitru, D., Nandedkar, S. D., and Netherton, B. (2010). "Neurophysiology and instrumentation," in *AANEM 57th Annual Meeting*, Québec, Canada.

Hari, R., Hällström, J., Tiihonen, J., and Joutsiniemi, S.-L. (1989). Multichannel detection of magnetic compound action fields of median and ulnar nerves. *Electroencephalogr. Clin. Neurophysiol.* 72, 277–280. doi: 10.1016/0013-4694(89)90253-8

Hashimoto, I., Mashiko, T., Mizuta, T., Imada, T., Iwase, K., and Okazaki, H. (1994). Visualization of a moving quadrupole with magnetic measurements

of peripheral nerve action fields. *Electroencephalogr. Clinic. Neurophysiol.* 93, 459–467. doi: 10.1016/0168-5597(94)90154-6

Hill, R. M., Boto, E., Rea, M., Holmes, N., Leggett, J., Coles, L. A., et al. (2020). Multi-channel whole-head OPM-MEG: helmet design and a comparison with a conventional system. *NeuroImage* 219:116995. doi: 10.1016/j.neuroimage.2020.116995

Iivanainen, J., Stenroos, M., and Parkkonen, L. (2017). Measuring MEG closer to the brain: performance of on-scalp sensor arrays. *NeuroImage* 147, 542–553. doi: 10.1016/j.neuroimage.2016.12.048

Jabre, J. F. (1981). Surface recording of the H-reflex of the flexor carpi radialis. *Muscle Nerve.* 4, 435–438. doi: 10.1002/mus.880040514

Jabre, J. F., and Stålberg, E. V. (1989). Single-fiber EMG study of the flexor carpi radialis H reflex. *Muscle Nerve.* 12, 523–527. doi: 10.1002/mus.880120702

Jin, X., Zhu, Y., Lu, F. Z., Wu, X. D., Zhu, D. Q., Weber, R., et al. (2010). H-reflex to S1-root stimulation improves utility for diagnosing S1 radiculopathy. *Clin. Neurophysiol.* 121, 1329–1335. doi: 10.1016/j.clinph.2010.03.004

Khosrawi, S., Vahdatpour, B., and Ahmadi, M. (2018). Evaluation of Relationship between Extensor Digitorum Communis Hoffmann-reflex Latency and Upper Limb Length and Age. *Advanced Biomedical Research* 7. doi: 10.4103/abr.abr_106_17.

Krarup, C. (2004). Compound sensory action potential in normal and pathological human nerves. *Muscle Nerve.* 29, 465–483. doi: 10.1002/mus.10524

Kronland-Martinet, R., Morlet, J., and Grossmann, A. (1987). Analysis of sound patterns through wavelet transforms. *Int. J. Pattern Recognit. Artif. Intell.* 1, 273–302. doi: 10.1142/S0218001487000205

Lang, G., Shahani, U., Weir, A., Maas, P., Pegrum, C., and Donaldson, G. (1998). Neuromagnetic recordings of the human peripheral nerve with planar SQUID gradiometers. *Phys. Med. Biol.* 43, 2379–2384. doi: 10.1088/0031-9155/43/8/027

Loic, Q. (2015). Biot Savart magnetic Toolbox. *Tech. Report, Dept. Elect. Eng.*, University of Applied Sciences Düsseldorf, Germany.

Mai, J. K., and Paxinos, G. (2011). *The Human Nervous System*. New York: Academic Press.

Merletti, R., Conte, L. L., and Sathyan, D. (1995). Repeatability of electrically-evoked myoelectric signals in the human tibialis anterior muscle. *J. Electromyogr. Kinesiol.* 5, 67–80. doi: 10.1016/1050-6411(94)00004-6

Shah, V., and Romalis, M. V. (2009). Spin-exchange relaxation-free magnetometry using elliptically polarized light. *Phys. Rev. A* 80:013416. doi: 10.1103/PhysRevA.80.013416

Shehab, D. K. (1998). Normative data of nerve conduction studies in the upper limb in Kuwait: are they different from the western data? *Med. Princ. Pract.* 7, 203–208. doi: 10.1159/000026043

Stowe, A. M., Hughes-Zahner, L., Stylianou, A. P., Schindler-Ivens, S., and Quaney, B. M. (2008). Between-day reliability of upper extremity H-reflexes. *J. Neurosci. Methods* 170, 317–323. doi: 10.1016/j.jneumeth.2008.01.031

Sulaiman, H., Gabella, G., Davis, C., Mutsaers, S. E., Boulos, P., Laurent, G. J., et al. (2001). Presence and distribution of sensory nerve fibers in human peritoneal adhesions. *Ann. Surg.* 234, 256–261. doi: 10.1097/00000658-200108000-00016

Valls-Sole, J., Leote, J., and Pereira, P. (2016). Antidromic vs orthodromic sensory median nerve conduction studies. *Clin. Neurophysiol. Pract.* 1, 18–25. doi: 10.1016/j.cnp.2016.02.004

Wang, J., She, S., and Zhang, S. (2002). An improved Helmholtz coil and analysis of its magnetic field homogeneity. *Rev. Sci. Instrum.* 73, 2175–2179. doi: 10.1063/1.1471352

Yang, J., Chen, K., Liu, Y., and Yang, Y. (2021). Prolonged median distal sensory nerve action potential duration in carpal tunnel syndrome. *Muscle Nerve* 63, 710–714. doi: 10.1002/mus.27190

Zheng, C., Zhu, Y., Lv, F., Ma, X., Xia, X., Wang, L., et al. (2014). Abnormal flexor carpi radialis H-reflex as a specific indicator of C7 as compared with C6 radiculopathy. *J. Clin. Neurophysiol.* 31, 529–534. doi: 10.1097/WNP.0000000000000104